BMC Nephrology

RESEARCH Open Access

FTO mediates the diabetic kidney disease progression through regulating the m^{6}A modification of *NLRP3*

Qiang Li[1] and Shujuan Mu[1*]

Abstract

Background The objective of our research was to investigate the specific mechanism of *FTO* in diabetic kidney disease (DKD) progression.

Methods The DKD model was established with renal tubular epithelial HK-2 cells and mice in vitro and in vivo. The N6-methyladenosine (m^{6}A) content in cells was detected using dot plot assay and the m^{6}A levels of *NLRP3* was detected with the MeRIP assay. The mRNA and protein levels were tested with real-time reverse transcriptase-polymerase chain reaction (RT-qPCR) and western blot. The IL-1β and IL-18 levels were assessed with enzyme-linked immunosorbent assay (ELISA). The cell viability was measured by cell counting kit (CCK)-8 assay and cell pyroptosis was determined with Annexin V and propidium iodide (PI) double staining followed by flow cytometry analysis. RNA-binding protein immunoprecipitation (RIP) and dual luciferase reporter assays were conducted to detect the interaction between *FTO* and *NLRP3*. m^{6}A levels were detected by Me-RIP assay. The renal injury was measured by observing the renal morphology and urine and blood levels of relevant indicators.

Results The results indicated that high glucose treatment induced HK-2 cell pyroptosis. m^{6}A levels were prominently elevated in high glucose treated HK-2 cells while *FTO* expression were significantly down-regulated. *FTO* over-expression promoted cell viability but inhibited pyroptosis of HK-2 cells under high glucose (HG) treatment. Moreover, *FTO* could inhibit *NLRP3* expression. RIP and Me-RIP assays indicated that *FTO* could bind with *NLRP3* and regulate its m^{6}A modification level. Further luciferase assay confirmed that *FTO* binds with the 233–237 bp region of *NLRP3*. *NLRP3* neutralized the function of *FTO* in the HG stimulated HK-2 cells. In vivo, the H&E staining showed that *FTO* over-expression alleviated the kidney injury and suppressed the pyroptosis induced by DKD.

Conclusion We found that *FTO* could inhibit the DKD progression in vivo and in vitro by regulated the m^{6}A modification of *NLRP3*.

Keywords Diabetic kidney disease, *FTO*, Pyroptosis, NLRP3, m^{6}A

*Correspondence:
Shujuan Mu
liqiang382169@sina.com
[1]Department of Nephrology, Guang'anmen Hospital South Campus, China Academy of Chinese Medical Sciences, No.138, Xingfeng Street, Huangcun Village, DaXing District, Beijing 102600, China

Introduction

Diabetic kidney disease (DKD) is a microvascular complication of diabetes [1]. DKD is characterized by the increase formation of extracellular matrix and disappearance of foot process, which eventually leads to increased urinary protein and decreased estimated glomerular filtration rate [2, 3]. Previous studies have shown that DKD is the result of the interaction of hemodynamic disorders and metabolic abnormalities [4]. However, increasing evidences have determined that the local inflammatory state of the kidney leads to the occurrence and progression of DKD [5]. In DKD patients, the driving effect of hyperglycemia, the increase of toxic metabolites (such as advanced glycation end), and the vascular mechanical changes caused by the disturbance of hemodynamics will lead to the inflammatory response in vivo, which further affect the proliferation, hypertrophy, aging and apoptosis of renal cells [6, 7].

In recent years, epigenetics, a branch of genetics, has developed rapidly. Epigenetics mainly regulates gene expression through gene modification, without changing the nucleotide sequence of the gene [8]. RNA modification widely affects the structure, function and stability of RNA, which plays a critical role in the regulation of various cell process [9]. Among all RNA modifications, N6 methyladenosine (m^6A) is the most common modification form in eukaryotic mRNA, which is also one of the most studied RNA modifications at present [10]. Fat-mass and obesity-associated gene (*FTO*) is a central enzyme in the process of methylation modification, which has been confirmed to be closely related to many diseases progression [11]. Additionally, abnormal *FTO* levels participate in the regulation of inflammation and cell death, which are critical mechanisms in the malignant development of DKD [12]. However, whether *FTO* modulates the development of DKD and its potential mechanism are largely unknown.

Pyroptosis is a newly identified programmed cell death characterized by cell swelling and information reaction. Recent researches demonstrate that the pyroptosis of renal tubular epithelial cell has been found in the process of DKD [13–15]. The NLRP3 inflammasome is known to be the most important initiator of pyroptosis [16]. Thus, controlling the activation of the NLRP3 inflammasome and podocyte pyroptosis play important roles in the progression of DKD. Here in this study, we aimed to investigate the effect and mechanism of *FTO* in DKD development. We hypothesized that *FTO* involves in the DKD progression through m^6A modification of *NLRP3* and regulating cell pyroptosis.

Materials and methods

Cell culture and treatment

Human renal tubular epithelial cell (HK-2) was provided by Shanghai Mingjin Biotechnology Co., Ltd (Shanghai, China). The cells were maintained in the endothelial culture medium supplemented with 5.6 mmol/L glucose and 10% fetal bovine serum (FBS; Gibco). In order to induce the DKD model, HK-2 cells were treated with 30 mmol/L d-glucose for 48 h, named high glucose (HG) group. In addition, HK-2 cells were treated with 5.6 mmol/L d-glucose in the normal glucose (NG) group, while cells cultured in 25 mM mannitol were used as the osmotic control (M group).

Cell transfection

FTO over-expressing vector (oe-FTO), *NLRP3* over-expressing vector (oe-NLRP3) and empty vector (oe-NC) were provided by GenePharma (Shanghai, China). In brief, pUC57-FTO and pLVX-mCMV-ZsGreen-IRES-Puro were digested by EcoRI and SpeI, and the products were connected by T4 DNA Ligase. Then, an Agarose Gel Extraction Kit was used to retrieve fragments. JM109, which was transfected with the ligation product, was inoculated and amplificated, and the sequencing primer CMV-F was used to verify the bacterial fluid. rLV-FTO/NLRP3 was obtained in 293T cells co-transfected with recombinant plasmid or control plasmid using Lipofectamine 3000 (Invitrogen, USA). HK-2 cells were transfected with rLV-FTO/NLRP3 on the basis of MOI = 20. Two days after transfection, lentivirus-infected HK-2 cells were cultured normally.

Real-time reverse transcriptase-polymerase chain reaction (RT-qPCR)

The total RNA was extracted with Trizol Kits (Beyotime, Shanghai, China), and the total RNA was reverse transcribed into cDNA according to the instructions of the PrimeScript RT reagent kit (Takara, Japan). The synthetic cDNA was used as the templates for the RT-qPCR reaction with a Fast SYBRGREEN PCR kit (Takara), and in a ABIPRISM 7300 RT-PCR system (Applied Biosystems). The amplification program was set as follows: initial denaturation, 95℃ for 15 min; denaturation, 95℃ for 15 s, 45 cycles; annealing, 55℃ for 15 s; extension, 72℃ for 30 s. In this experiment, *β-actin* was used as the internal control of genes. Relative quantification method ($2^{-\Delta\Delta Ct}$ method) was used to calculate the relative levels of related genes. The primer sequences were as follows: *FTO*, 5′-GCTGCTTATTTCGGGACCTG-3′ and 5′-AGCCTGGATTACCAATGAGGA-3′; *NLRP3*, 5′-CCACAAGATCGTGAGAAAACCC-3′ and 5′-CGGTCCTATGTGCTCGTCA-3′;

CASP1, 5′-TTTCCGCAAGGTTCGATTTTCA-3′ and 5′-GGCATCTGCGCTCTACCATC-3′; *ASC*, 5′-CCCAAGCAAGTCAAGCGACA-3′ and 5′-AAGCCGCTGAAGTTGAGCC-3′; *GSDMD*, 5′-GGACAGGCAAAGATCGCAG-3′ and 5′-CACTCAGCGAGTACACATTCATT-3′; and GAPDH, 5′-GTGTTCCTACCCCCAATGTGT-3′ and 5′-ATTGTCATACCAGGAAATGAGCTT-3′.

RNA stability detection

For the determination of mRNA stability of *NLRP3*, the cells were treated with Actinomycin D for 2, 4, 6, 8 h. After the treatment of different times, the mRNA levels of *NLRP3* were detected using RT-qPCR as mentioned above.

Cell counting kit (CCK)-8 assay

CCK-8 detection kit (Shanghai Liji Biotechnology Co., Ltd., Shanghai, China) was used to detect the cell viability. 100 μL of cell suspension was seeded in a 96-well plate at a density of 5×10^3/well. On the 24th, 48th, and 72th h after seeding, 10 μL of CCK-8 solution was added to each well, and mixed gently without bubbles. After incubated in a 5% CO_2 incubator at 37 ℃ for 4 h, the absorbance of each well at 450 nm was measured with a microplate reader.

Annexin V and propidium iodide (PI) double staining

Pyroptosis of HK-2 cells was detected by using an Annexin V-FITC Detection Kit (Beyotime) according to the manufacturer's instructions. Briefly, HK-2 cells at the concentration of 2×10^5 were centrifuged at 300 × g for 5 min, and the supernatant was discarded. The cells were re-suspended with 500 μL diluted 1 × Annexin V Binding Buffer. The cell suspension was added with 5 μL Annexin V-FITC staining solution and 5 μL PI staining solution (50 μg/mL). Cells ere incubated at room temperature for 15 ~ 20 min away from light, and then analyzed by flow cytometry (Becton Dickinson, Germany). HK-2 cells in Q1 (Annexinv-/PI+) are necrotic cells [17], and were deemed as positive pyroptosis cells.

Western blot

The cultured cells were collected and the supernatant was discarded. Then the cells were lysed with enhanced RIPA lysate (Beyotime), and the protein concentration was determined with BCA protein quantitative Kit (Beyotime). Proteins (20 μg) were separated with 10% SDS-PAGE and transferred to PVDF membrane (Millipore). Membranes were blocked in 5% skimmed milk at room temperature for 1 h. Then the blots were treated with primary antibodies against (NLRP3, 27458-1-AP, Proteintech, China; ASC, ab307560, Abcam, USA; caspase-1, ab286125, Abcam, USA; GSDMD-N, EPR20829-408, Abcam, USA; IL-6, ab290735, Abcam, USA; caspase-3, ab32351, Abcam, USA) at 4℃ overnight. Next day, after washing, the membranes were treated with HRP labeled secondary antibody for 1 h. Thereafter, the membranes were visualized with ECL solution (Biomiga, USA) for 1 min at room temperature. ImageJ software was used to quantify the gray scale of each band. β-actin was used as the internal control.

m6A dot blot assay

Total RNA was extracted from the blood, cells and tissues by Trizol (Beyotime). The m^6A content relative to the total mRNA level was measured by EpiQuik m^6A RNA Methylation Quantification Kit (Colorimetric) (AmyJet Scientific, Wuhan, China) according to the instructions. Briefly, 4 μg of total RNA was and purified using the RNeasy Mini Kit (Qiagen). Then the RNA was separated on 1.2% formaldehyde-agarose gels and transferred onto Hybond *N*+membranes (Amersham). Then the membranes were incubated with m^6A antibody overnight and and then treated with horseradish peroxidase conjugate anti-rabbit immunoglobulin G. Finally, after washing, the blots were developed on PhosphorImager screens and quantited with ImageQuant.

Me-RIP qPCR experiment

Magna RIPTM RNA binding protein immunoprediction kit was purchased from Millipore (MA, USA) and the experiment was carried out according to the instructions. After the cells were treated with Rip lysate, anti-m^6A antibody was used to incubate the cell lysate. Then the mixture was incubated with magnetic beads. After that, protease K was used to remove proteins. Finally, the RNA was purified and reverse transcribed into cDNA, and the expression of target genes was detected by RT-qPCR.

RNA-binding protein immunoprecipitation (RIP) experiment

The Rip Kit (Millipore, USA) was used to detect the binding of FTO protein with *NLRP3* RNA. HK-2 cells were washed twice with cold PBS and collected. The cells were then resuspended with RIPA lysate (Beyotime) and centrifuged (14 000 r/min, 4 ℃) for 10 min to collect the supernatant. The experimental procedures were as follows: 50 μL of magnetic beads were washed and then resuspended in 100 μL of RIP Wash Buffer, and then incubated with 5 μg of anti-FTO or IgG. The magnetic bead-antibody complexes were washed and resuspended in 900 μL RIP Wash Buffer, and then incubated with 100 μL cell extract at 4℃ overnight. The sample was then placed on a magnetic

holder to collect the magnetic bead-protein complexes. The complex pulled down were digested with proteinase K to extract RNA, and the expression level of *NLRP3* was detected by RT-qPCR as mentioned above.

Double luciferase reporter assay

The wild-type and mutant fragments of *NLRP3* were constructed and inserted into the pmirGLO reporter vector using endonuclease sites Spe I and Hind III, named as NLRP3-WT and NLRP3-MUT, respectively. These reporter plasmids along with oe-nc or oe-FTO were co-transfected into HK-2 cells using the LipofectamineTM3000 reagent. After 48 h, the cells were collected and fully lysed. The firefly luciferase activity was finally measured and normalized to the renin luciferase activity.

Animal experiment

The experimental procedures followed the recommendations in the Guide for the Care and Use of Laboratory Animals published by the National Institutes of Health and were approved by Laboratory Animal Ethics Committee of the Beijing Medconor Biotechnology Co., LTD. (MDKN-2022-70). Five weeks old male C57bl/6 mice (20 ± 2 g) were divided into DKD model group and control group. The fasting blood glucose of all mice was measured before the experiment, which was required to be less than 7 mmol/L. The mice in DKD model group were fed with high-fat and high-glucose diet for 8 weeks. Then, 1 day after restoring the high-fat and high-glucose diet, the mice in the DKD model group were fasted for 16 h and injected with streptozotocin (STZ) at 50 mg/kg per day for 5 days. The fasting blood glucose was measured 2 weeks after the last injection. If the fasting blood glucose was greater than 16 mmol/L, the medium-term diabetes model was established successfully. The mice in the control group were received standard chow and injected with the same amount of normal saline. Subsequently, all DKD mice were randomly divided into lv-NC group and lv-FTO group. After DKD model establishment, the lentiviruses carrying empty vector (NC) or *FTO* over-expressing vector (FTO) (MOI = 50) were injected into caudal vein at the dose of 1 μg/g according to the weight of mice, once a week for 8 weeks.

H&E staining

Mice were sacrificed with 160 mg/kg pentobarbital sodium injection to cause respiratory arrest. The kidneys of the mice were collected and fixed in 4% paraformaldehyde. After the fixation, dehydration and paraffin embedding, the paraffin sections were cut into sections with a thickness of 2 μm. H&E staining kit were purchased from Shanghai GEFAN Biotechnolog Co., Ltd. (Shanghai, China). The sections were stained according to the instructions of the kits. The pathological changes of renal glomerulus, basement membrane and mesangial matrix were observed under the microscope. The renal tubule injury was evaluated as described previously [18].

Detection of renal tubule injury

The IL-1β, IL-18 and LDH levels in the kidneys of the mice and the HK-2 cells were tested by corresponding ELISA kits purchased from Jiancheng Bio (Nanjing, China). All operations shall be carried out according to the operation instructions of the kits. Urine samples were collected from the metabolic cage 2 days before sacrifice, and the urinary albumin level and urinary albumin excretion rate (mg/24 h) were measured according to the instructions of enzyme-linked immunosorbent assay (ELISA) kit (Ethos Biosciences). Femoral vein blood was collected with heparin anticoagulation capillary tubes for measurement of blood urea nitrogen, serum creatinine and glomerular filtration rate using biochemical analyzer (Mindray). To measure urinary N-acetyl-beta-D-glucosidase (NAG) and retinol-binding protein-4 (RBP-4) levels, particle-enhanced turbidimetric immunoassay (PETIA) kits (Diazyme, USA) were implemented.

Statistical analysis

SPSS 22.0 software was applied for data analysis. The results were expressed by mean ± SD. The independent sample T-test was used for the comparison between the two groups, and the one-way ANOVA was used for the comparison between multiple groups. The m^6A methylation sites of *NLRP3* were predicted using the SRAMP database (http://www.cuilab.cn/sramp). $P < 0.05$ was statistically significant.

Results

HG induced pyroptosis and elevated the m6A level of renal tubular epithelial cells

After HG treatment, cell viability of HK-2 cells was suppressed compared with NG and M groups (Fig. 1A). The LDH release in the culture medium of HK-2 cells was also significantly increased (Fig. 1B). Flow cytometry results indicated that HG notably induced pyroptosis of HK-2 cells. ELISA results showed that HG promoted the release of IL-1β and IL-18 of HK-2 cells (Fig. 1C, D, E). Western blot was used to assess the protein expression. It was showed that HG promoted the expression of NLRP3, ASC, cleaved caspase-1, caspase-3 and GSDMD-N (Fig. 1F, Fig. S1A). These results demonstrated that HG could induce pyroptosis

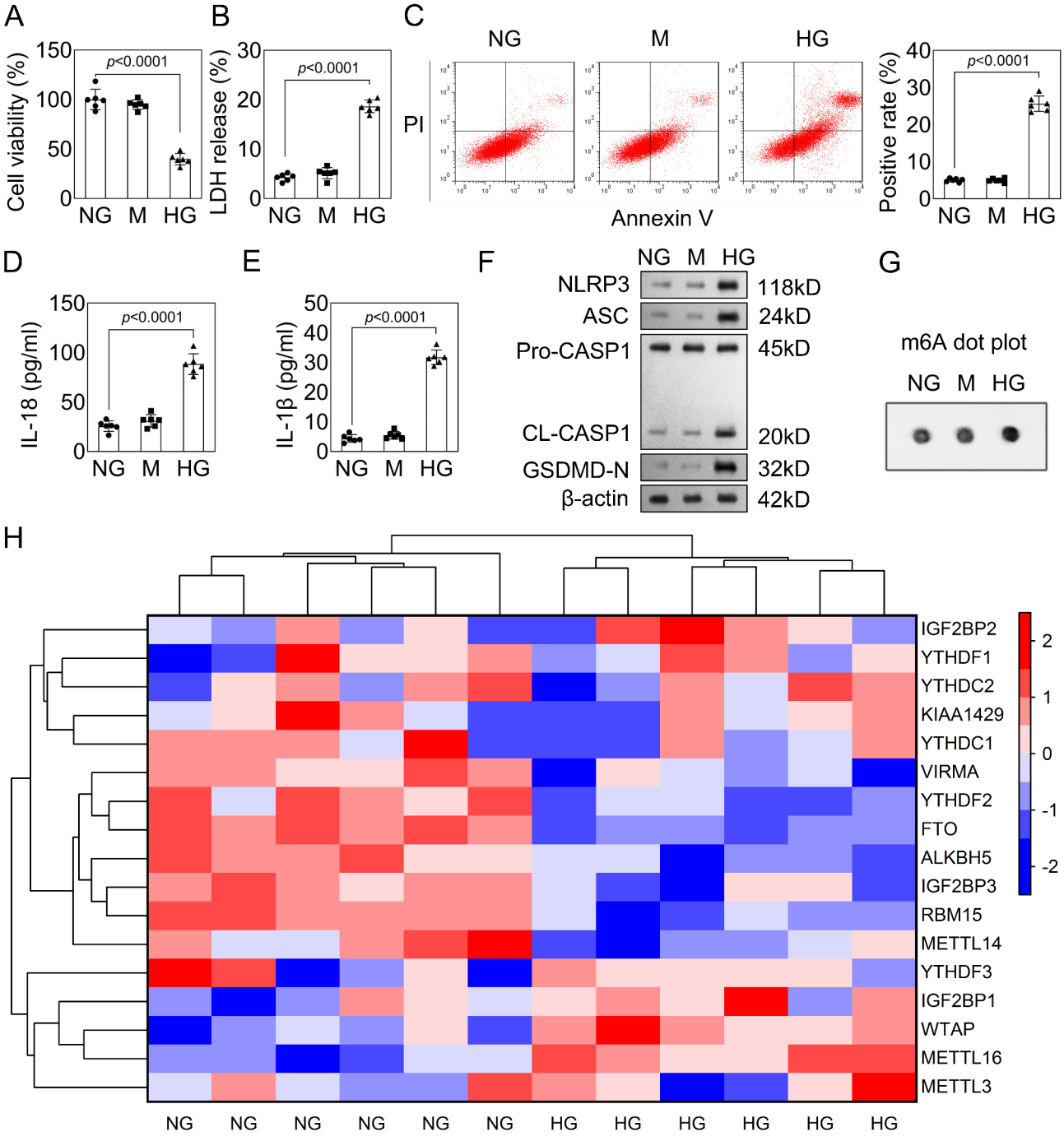

Fig. 1 (**A**) Cell viability was assessed by CCK-8 after HG treatment. (**B**) LDH release in HK-2 cell culture medium was determined by commercial kits. (**C**) The pyroptosis of HK-2 cells was detected by flow cytometry. (**D**) The release of IL-1β and IL-18 in HK-2 cells was assessed. (**F**) HG promotes protein expression of NLRP3, ASC, cleared caspase-1 and GSDMD-N. (**G**) m6A dot plot staining was performed to evaluate the level of m6A in HK-2 cells. (**H**) The expressions of m6A related regulatory factors were detected by qPCR in HK2 cells after HG treatment. The one-way ANOVA was used for the comparison between multiple groups, and data were expressed by mean ± SD

of HK-2 cells in vitro. Subsequently, we investigated whether HG could influence the m^{6}A level. Dot plot staining showed that HG did elevate the m6A level of HK-2 cells (Fig. 1G). The performance of HK-2 cells treated with mannitol was not statistically different from that of the NG group. Then, we tried to figure out which m^{6}A related regulators lead to the abnormal m^{6}A level of DKD. The results suggested that the *FTO* level was prominently decreased in the HG stimulated

HK-2 cells (Fig. 1H). Thus, we selected *FTO* for the further study.

Over-expression of *FTO* alleviated the injury in HK-2 cells induced by HG treatment

Then, we constructed *FTO* over-expressing vectors. The qPCR results confirmed that oe-FTO successfully elevated the *FTO* level in HK-2 cells (Fig. 2A). HG treatment dramatically suppressed the cell viability of the HK-2 cells, while oe-FTO significantly enhanced it (Fig. 2B). The promoted release of LDH was reversed by *FTO*, either (Fig. 2C). Besides, HG treatment dramatically elevated the pyroptosis rate of HK-2 cells while *FTO* reduced it (Fig. 2D). In addition, *FTO* inhibited the HG promoted release of IL-1β and IL-18 (Fig. 2E, F) and the expression of NLRP3, ASC, cleaved caspase-1, caspase-3 and GSDMD-N (Fig. 2G, Fig. S1B).

FTO regulated m^{6}A modification of *NLRP3*

As F*TO* participates in the regulation of pyroptosis, we are wondering whether *FTO* could regulate the m^{6}A modification of pyroptosis related genes. The Me-RIP assay indicated that *FTO* could significantly reduce the m^{6}A level of *NLRP3* but not that of caspase-1, ASC or GSDMD (Fig. 3A). Furthermore, the RIP assay showed that the FTO antibody could enriched the *NLRP3* mRNA in HK-2 cells (Fig. 3B). After *FTO* over-expression, the m^{6}A levels of *NLRP3* were prominently decreased (Fig. 3C). Then, SRAMP, a sequence-based m^{6}A modification site predictor, was applied to predict the potential theoretical binding sites of *NLRP3*, and there are 3 site for m^{6}A modification located at 233–237, 866–870 and 1404–1408 bp (Fig. 3D). Afterwards, whether the site can play the m^{6}A modification function is verified by the base mutation of the binding site (Fig. 3E). The luciferase assay indicated that *FTO* prominently reduced the luciferase activity of WT-NLRP3 carrying 233–237 bp region but not MUT-NLRP3 (Fig. 3F). qPCR results indicated that *FTO* over-expression reduced the stability of *NLRP3* mRNA (Fig. 3G).

NLRP3 over-expression neutralized the function of *FTO* in the HG stimulated HK-2 cells

Finally, to confirm the interaction between *FTO* and *NLRP3*, the rescue experiments were conducted. We established the *NLRP3* over-expressing vector and found that it prominently elevated the mRNA expression of *NLRP3* in HK-2 cells (Fig. 4A). *NLRP3* over-expression prominently decreased the cell viability (Fig. 4B), but elevated the LDH release (Fig. 4C). Pyroptosis rate and IL-1β and IL-18 amount were elevated by *NLRP3* over-expression (Fig. 4D-F). Additionally, after *NLRP3* over-expression, the protein expressions of NLRP3, ASC, cleaved caspase-1, caspase-3 and GSDMD-N were promoted (Fig. 4G, Fig. S1C). These results further confirmed the interaction between *FTO* and *NLRP3*.

Over-expression of *Fto* inhibited the DKD progression in vivo

Next, we focused our interest on renal tubular function and evaluated the potential protective roles of over-expression of *Fto* against DKD. The ratio of kidney weight to body weight was increased with exposure to STZ, and this trend was altered by over-expression of *Fto*. Meanwhile, STZ treatment resulted in a remarkable renal tubular injury as evidenced by increased urinary albumin, blood urea nitrogen, serum creatinine, glomerular filtration, 24 h urinary albumin excretion rate, NAG and RBP-4 levels. However, the application of elevated *Fto* greatly reduced these metabolites (Table 1). Then the pathologic changes of renal tissues were observed by H&E staining. Remarkable renal damage with many dilated and atrophic tubules were observed in DKD group, and over-expression of *Fto* significantly alleviated the above renal damages (Fig. 5A). The increased abundance of renal IL-6 was also down-regulated by elevated *Fto* (Fig. 5A). Meanwhile, the kidney damage injury was evaluated based on the results of H&E staining, and the data demonstrated that elevation of *Fto* significantly down-regulated the scores induced by DKD (Fig. 5B). Then, to check if *Fto* over-expression influence the pyroptosis, we evaluated the expression of pyroptosis related proteins. The results indicated that *Fto* over-expression inhibited the amount of IL-1β, IL-18 and the expression of NLRP3, ASC, cleaved caspase-1, caspase-3 and GSDMD-N (Fig. 5C-E, Fig. S1D).

Discussion

In the present research, we demonstrated that *FTO* inhibited the *NLRP3* expression via m6A modification. Additionally, we illustrated that *FTO* was prominently lowly expressed in HK-2 cells treated by HG. *FTO* over-expression relieved the injury of HK-2 cells induced by HG treatment and repressed the kidney injury in the DKD mice. This research is the first to investigate the function of *FTO* on the *NLRP3* signaling mediated pyroptosis in DKD progression.

Identifying targets for therapeutic interventions is critical to developing strategies to combat the development and progression of DKD disease [19]. Accumulating evidence suggested that the mainstay treatments of DKD including renin-angiotensin system inhibitors, sodium-glucose co-transporter 2 inhibitors, incretin-based therapeutic agents, and non-steroidal

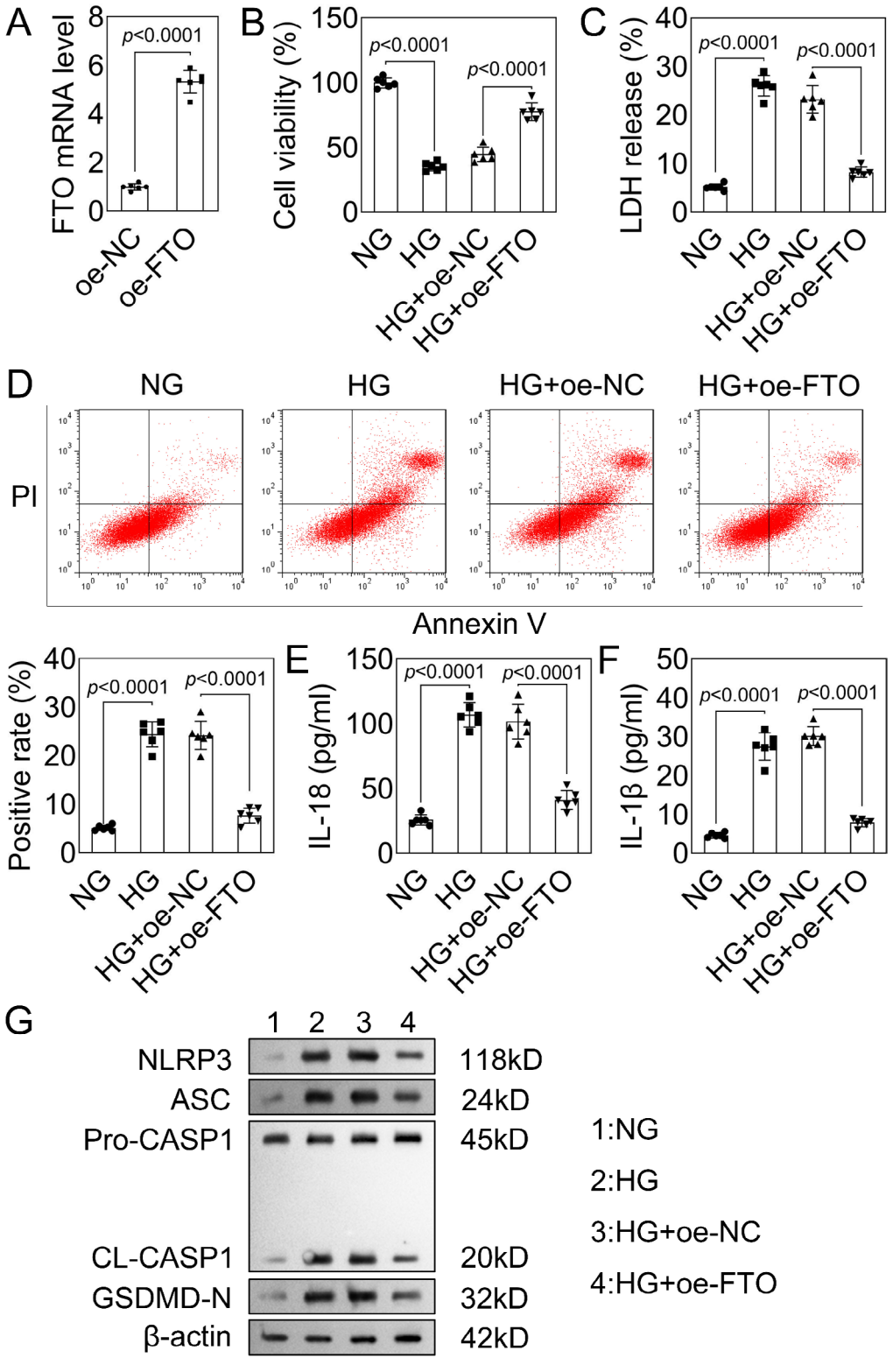

Fig. 2 FTO over-expression moderated the injury in the HK-2 cells induced by HG treatment. (**A**) The expression of *FTO* after transfection was evaluated by RT-qPCR. oe-FTO successfully increased the level of *FTO* in HK-2 cells. (**B**) Cell viability after treatment and transfection was assessed by CCK-8. (**C**) Promoted release of LDH. (**D**) Flow cytometry was used to evaluate the pyroptosis of HK-2 cells. (**E**) *FTO* inhibited the HG promoted release of IL-1β (**F**) and IL-18. (**G**) The expression of NLRP3, ASC, cleaved caspase-1 and GSDMD-N. The independent sample T-test was used for the comparison between the two groups, and the one-way ANOVA was used for the comparison between multiple groups. The data were expressed by mean ± SD

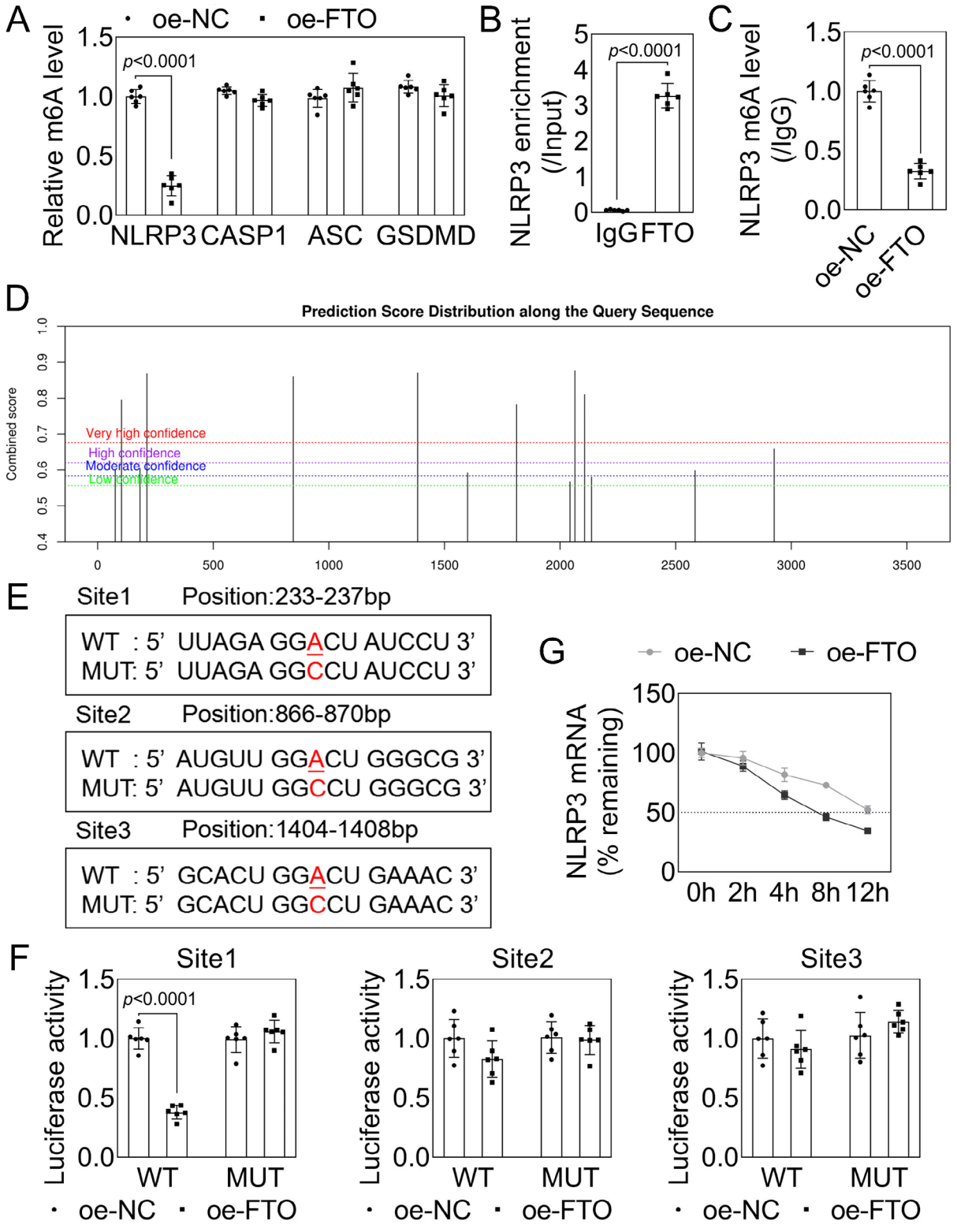

Fig. 3 FTO over-expression moderated the DKD progression in vivo. (**A**) m6A level of NLRP3, caspase-1, ASC and GSDMD. (**B**) RIP assay was performed to detect the binding of *FTO* with *NLRP3* mRNA. (**C**) m6A level of *NLRP3* after *FTO* knockdown was detected. (**D**) Prediction of potential m6A modification sites of *NLRP3*. (**E**) The wild type (WT) and mutant (mut) sequence was showed. (**F**) Luciferase activity of WT-NLRP3 and MUT-NLRP3 after *FTO* over-expression was assessed. (**G**) The half life of *FTO* mRNA after *FTO* over-expression was detected by qPCR. The independent sample T-test was used for the comparison between the two groups, and the one-way ANOVA was used for the comparison between multiple groups. The data were expressed by mean ± SD

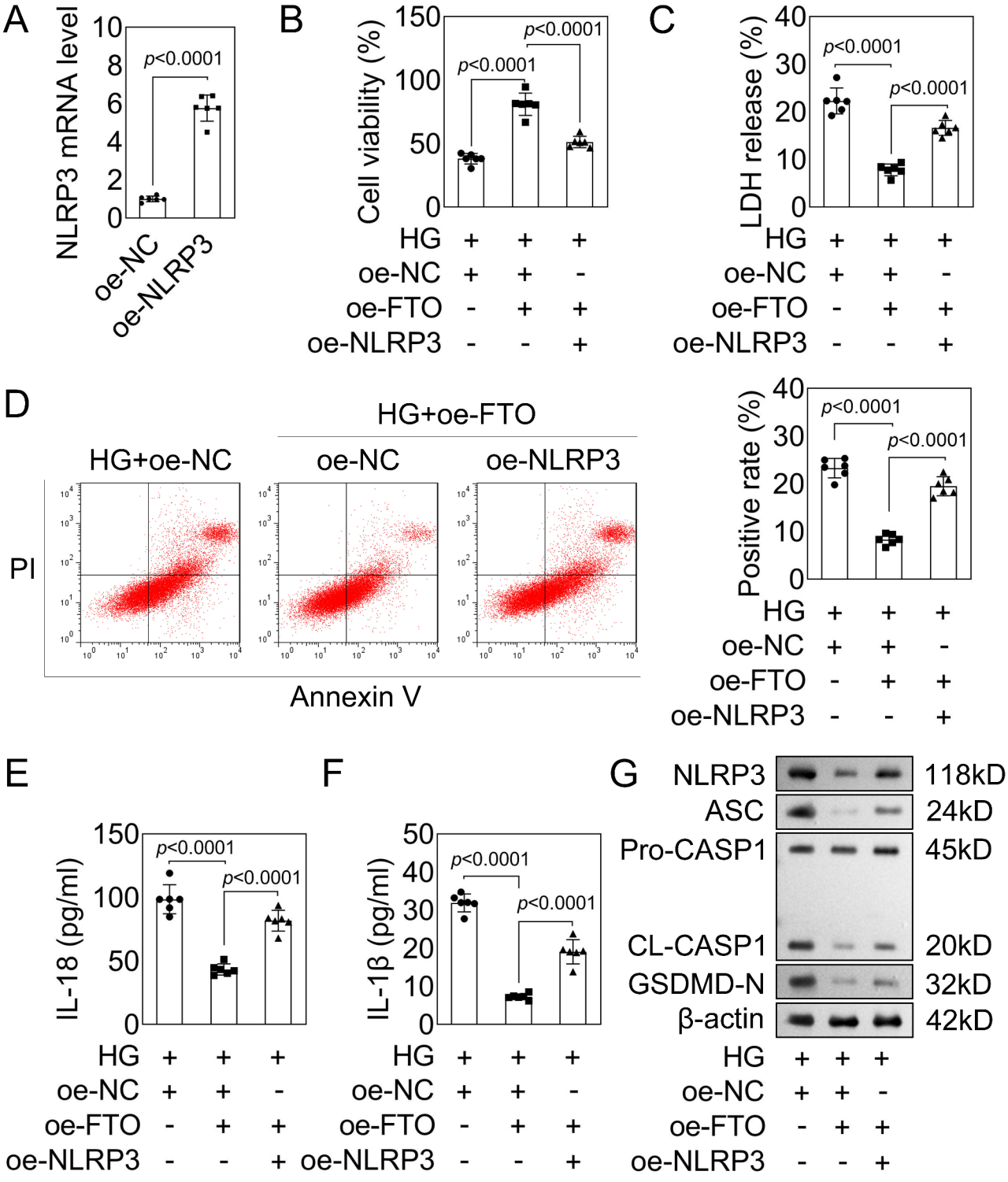

Fig. 4 FTO regulated m6A modification of *NLRP3*. (**A**) The *NLRP3* levels were measured by RT-qPCR in HK-2 cells. Over-expression of *NLRP3* reversed the effect of FTO on the (**B**) proliferation, (**C**) LDH release, (**D**) pyroptosis rate, (**E**, **F**) IL-18 and IL-1β release of HK-2 cells. (**G**) The effect of *FTO* on expression of NLRP3, ASC, cleared caspase-1 and GSDMD-N protein was reversed by *NLRP3* over-expression. The independent sample T-test was used for the comparison between the two groups, and the one-way ANOVA was used for the comparison between multiple groups. The data were expressed by mean ± SD

Table 1 Effects of overexpression of FTO on renal function in DKD model mice

	NC	DN	DN + lv-NC	DN + lv-FTO
Kidney weight/ Body weight	0.82 ± 0.06	0.99 ± 0.07**	1.01 ± 0.09	0.87 ± 0.09#
Urinary albumin level (mg/mg Ucr)	6.38 ± 0.79	31.71 ± 3.25**	34.07 ± 2.80	17.64 ± 2.45##
Blood urea nitrogen (mmol/L)	6.99 ± 0.50	12.90 ± 1.10**	13.22 ± 0.87	7.17 ± 0.51##
Serum creatinine (μmol/L)	7.46 ± 0.71	14.30 ± 0.91**	14.55 ± 0.86	9.47 ± 0.85##
Glomerular filtration rate (μl/min)	184.31 ± 16.33	244.37 ± 24.62**	252.03 ± 17.12	206.45 ± 18.37##
Urinary albumin excretion rate (mg/24 h)	0.48 ± 0.06	3.04 ± 0.23**	3.08 ± 0.16	1.51 ± 0.12##
NAG (U/24 h)	0.17 ± 0.04	0.35 ± 0.04**	0.36 ± 0.04	0.22 ± 0.04##
RBP−4 (mg/L)	10.64 ± 1.79	31.70 ± 7.12**	31.86 ± 4.76	21.05 ± 3.75##

Note: **$p < 0.01$ compared with the DN group, #$p < 0.05$, ##$p < 0.01$ compared with DN + lv-NC group

mineralocorticoid receptor antagonists have been reported to treat DKD with different targets [20, 21]. Despite the many advances in the clinical management of DKD, the number of cases of diabetic kidney disease continues to increase, in part, owing to a pandemic increase of people with diabetes [19]. It is of great significance to find new therapeutic targets for DKD, and the combination of new targets and existing therapeutic methods may be more helpful for the treatment of DKD.

m6A methylation is confirmed to be the most common RNA modification in mammals and is involved in the RNA metabolism processes including, such as RNA biosynthesis and decay [22, 23]. Demethylase *FTO*, as an important m6A regulator, has been highlighted to participate in various diabetic complications, including microvascular complication [24], diabetic cataract [25], diabetic foot ulcers [26]. Due to the different modification sites and m6A binding readers, the function of m6A modification is complex. For instance, Xu et al. [27] found that methylase *METTL14* levels were prominently depleted in the HK-2 cells after HG treatment, which would further inhibited the histone deacetylase 5 and TGF-β1 expression levels. Eventually affecting the EMT of renal tubular cells in DKD. However, Li et al. [28] suggested that *METTL14* levels were dramatically up-regulated in kidneys of DKD, which was further demonstrated to elevate the ROS, TNF-α and IL-6 levels in the regulation of m6A levels. Here, we confirmed that *FTO* was lowly expressed in DKD. *FTO* over-expression promoted the cell growth while inhibited the cell pyroptosis in vivo and in vitro. These findings are similar to the previous report of Jiang et al. [12], who also confirmed *FTO* silencing effectively relieved the podocyte injury in DKD mice. All these results implied that *FTO*-mediated m6A modification might be a critical factor in DKD progression. We found that *FTO* was dysregulated in the serum of DKD patients. In this study, we evaluated the protective effect of *FTO* on the kidneys in vivo by detecting changes in interleukin markers and pyroptosis related protein levels throughout the kidney tissue. However, whether this protective effect is accurately located in the renal tubules and glomeruli deserves further study. Moreover, we did not evaluate whether *FTO* could be the biomarker for the diagnose of DKD. It will be also studied in our further research.

Autophagy is a protective mechanism for maintaining cellular homeostasis, and impairment of autophagy can aggravate renal cell dysfunction and apoptosis [29]. In the microenvironment of diabetes, autophagy deficiency can induce the pathological changes of different renal cells and further promote the progression of renal disease [30–32]. Mitochondrial autophagy termed as mitophagy was discovered to decline the release of ROS, promote apoptotic substances and reduce apoptosis [33], and the increases of inflammatory cytokines and ROS have also been shown in DKD [34]. Recently, mitophagy mediated by NLRP3/Parkin signaling pathway has been proved to participate in various diseases and is the main pathway for the removal of damaged mitochondria [35, 36]. In this study, the western blot results revealed that in the HG-stimulated HK-2 cells, the ratio of LC3-II/LC3-I was prominently down-regulated, while p62 was up-regulated. *FTO* silencing reversed the effect of HG treatment. Additionally, we found that NLRP3/Parkin signaling pathway was inhibited in the HG-stimulated HK-2 cells. After *FTO* silencing, it was activated. Therefore, we speculate whether *FTO* regulates the signaling pathway by regulating the m6A methylation modification of *NLRP3*.

Interestingly, through the RIP and dual luciferase report assay, we confirmed the interaction between

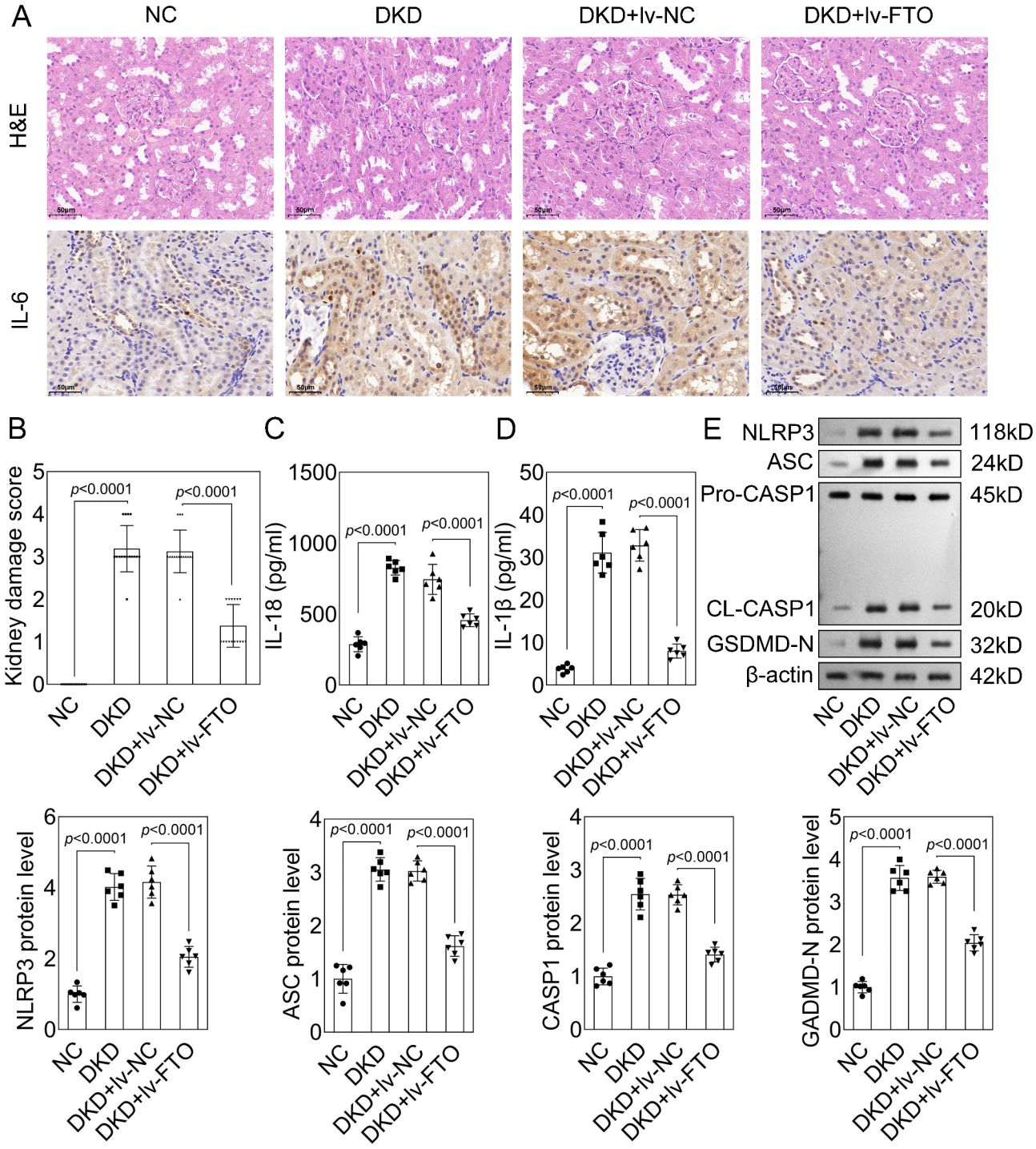

Fig. 5 Over-expression of *FTO* inhibited the DKD progression in vivo. (**A**) H&E staining and renal IL-6 levels evaluated by immunoblotting were performed to evaluate the effect of *FTO* on the kidney injury induced by high-fat and high-glucose diet. (**B**-**D**) ELISA was performed to detect the amount of IL-1β and IL-18 in the kidney tissue. (**E**) Expression of pyroptosis related proteins including NLRP3, ASC, cleared caspase-1 and GSDMD-N was evaluated by western blot. The one-way ANOVA was used for the comparison between multiple groups. The data were expressed by mean ± SD

FTO and *NLRP3*. And *FTO* silencing prominently decreased the m6A levels of *NLRP3* and increased the production of *NLRP3* mature mRNA levels. Furthermore, *NLRP3* silencing neutralized the functions of sh-FTO in the HG-stimulated HK-2 cells. These results indicated that *FTO* participated in the DKD progression through modulating the NLRP3/Parkin signaling pathway.

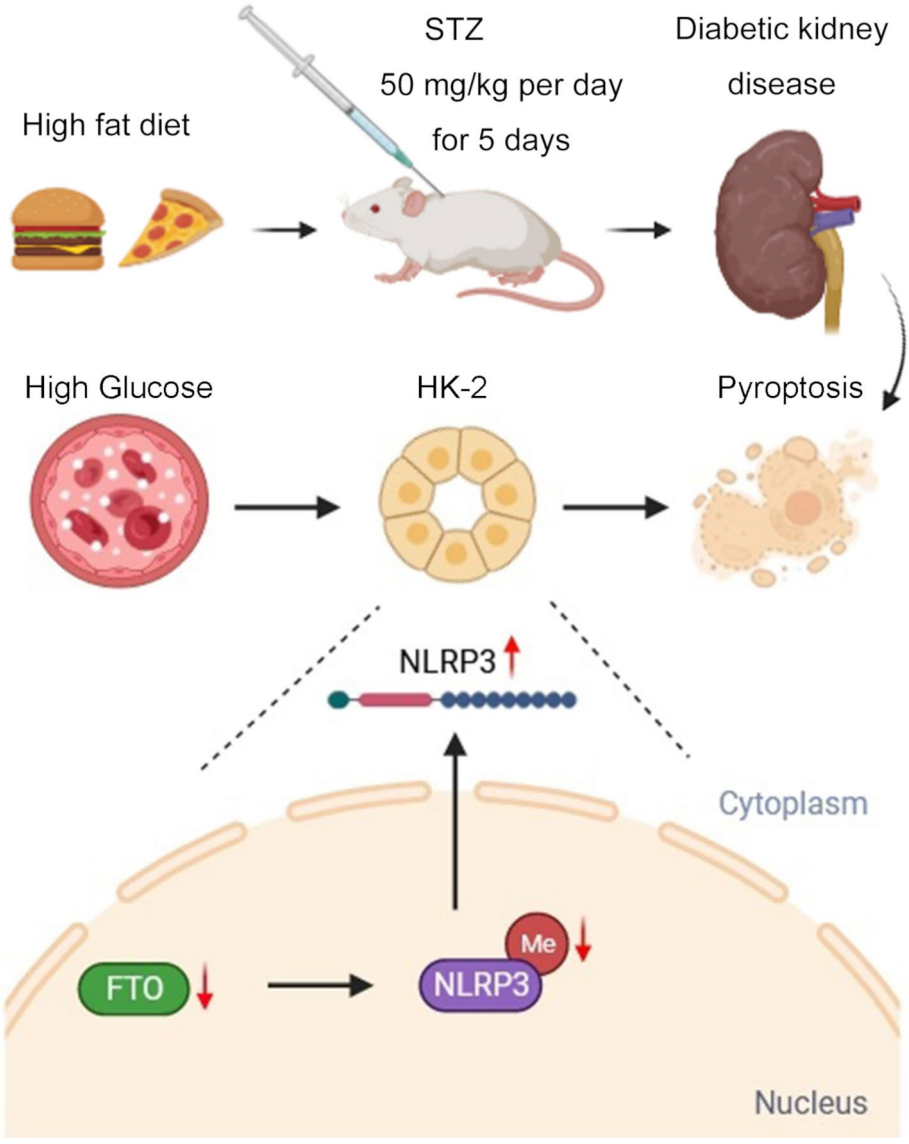

Fig. 6 Mechanism diagram

To sum up, our study determined that *FTO* mediates the DKD progression through regulating the pyroptosis of renal tubular epithelial cells. Mechanistically, *FTO* regulates the m6A modification and expression of *NLRP3* (Fig. 6). We hope these findings could provide novel targets for the treatment of DKD disease.

Supplementary Information

The online version contains supplementary material available at https://doi.org/10.1186/s12882-024-03741-5.

Supplementary Material 1
Supplementary Material 2
Supplementary Material 3
Supplementary Material 4
Supplementary Material 5
Supplementary Material 6
Supplementary Material 7
Supplementary Material 8
Supplementary Material 9
Supplementary Material 10
Supplementary Material 11
Supplementary Material 12
Supplementary Material 13
Supplementary Material 14
Supplementary Material 15
Supplementary Material 16
Supplementary Material 17
Supplementary Material 18

Supplementary Material 19

Supplementary Material 20

Supplementary Material 21

Supplementary Material 22

Supplementary Material 23

Supplementary Material 24

Supplementary Material 25

Supplementary Material 26

Supplementary Material 27

Supplementary Material 28

Supplementary Material 29

Supplementary Material 30

Supplementary Material 31

Supplementary Material 32

Supplementary Material 33

Supplementary Material 34

Acknowledgements
Not applicable.

Author contributions
Q L drafted the work and revised it critically for important intellectual content and was responsible for the acquisition, analysis and interpretation of data for the work; S M made substantial contributions to the conception or design of the work. All authors read and approved the final manuscript.

Funding
The authors declare that no funds, grants, or other support were received during the preparation of this manuscript.

Data availability
The datasets used and analyzed during the current study are available from the corresponding author on reasonable request.

Declarations

Ethics approval and consent to participate
All experimental protocols were approved by approved by Laboratory Animal Ethics Committee of the Beijing Medconor Biotechnology Co., LTD. (MDKN-2022-70). All methods are reported in accordance with ARRIVE guidelines (https://arriveguidelines.org) for the reporting of animal experiments. All methods were performed in accordance with the Basel Declaration.

Consent for publication
Not applicable.

Competing interests
The authors declare no competing interests.

Received: 23 August 2023 / Accepted: 3 September 2024
Published online: 11 October 2024

References

1. Papadopoulou-Marketou N, Paschou SA, Marketos N, Adamidi S, Adamidis S, Kanaka-Gantenbein C. Diabetic nephropathy in type 1 diabetes. Minerva Med. 2018;109(3):218.
2. Thipsawat S. Early detection of diabetic nephropathy in patient with type 2 diabetes mellitus: a review of the literature. Diab Vasc Dis Res. 2021;18(6):1476901544.
3. Sagoo MK, Gnudi L. Diabetic nephropathy: an overview. In., vol. 2067. New York, NY: Springer US; 2019: 3–7.
4. Geng XD, Wang WW, Feng Z, Liu R, Cheng XL, Shen WJ, Dong ZY, Cai GY, Chen XM, Hong Q, et al. Identification of key genes and pathways in diabetic nephropathy by bioinformatics analysis. J Diabetes Invest. 2019;10(4):972–84.
5. Wada J, Makino H. Innate immunity in diabetes and diabetic nephropathy. Nat Rev Nephrol. 2016;12(1):13–26.
6. Rayego-Mateos S, Morgado-Pascual JL, Opazo-Ríos L, Guerrero-Hue M, García-Caballero C, Vázquez-Carballo C, Mas S, Sanz AB, Herencia C, Mezzano S, et al. Pathogenic pathways and therapeutic approaches targeting inflammation in diabetic nephropathy. Int J Mol Sci. 2020;21(11):3798.
7. An X, Zhang Y, Cao Y, Chen J, Qin H, Yang L. Punicalagin protects diabetic nephropathy by inhibiting pyroptosis based on TXNIP/NLRP3 pathway. Nutrients. 2020;12(5).
8. Kaliman P. Epigenetics and meditation. Curr Opin Psychol. 2019;28:76–80.
9. Teng PC, Liang Y, Yarmishyn AA, Hsiao YJ, Lin TY, Lin TW, Teng YC, Yang YP, Wang ML, Chien CS et al. RNA modifications and epigenetics in modulation of lung cancer and pulmonary diseases. Int J Mol Sci. 2021;22(19).
10. Zhu W, Wang JZ, Xu Z, Cao M, Hu Q, Pan C, Guo M, Wei JF, Yang H. Detection of N6methyladenosine modification residues (review). Int J Mol Med. 2019;43(6):2267–78.
11. Chen M, Wei L, Law CT, Tsang FH, Shen J, Cheng CL, Tsang LH, Ho DW, Chiu DK, Lee JM et al. RNA N6-methyladenosine methyltransferase-like 3 promotes liver cancer progression through YTHDF2-dependent posttranscriptional silencing of SOCS2. Hepatology. 2018;67(6):2254–2270.
12. Jiang L, Liu X, Hu X, Gao L, Zeng H, Wang X, Huang Y, Zhu W, Wang J, Wen J, et al. METTL3-mediated m(6)a modification of TIMP2 mRNA promotes podocyte injury in diabetic nephropathy. Mol Ther. 2022;30(4):1721–40.
13. Zhou J, Wang C, Zhang X, Wu Z, Wu Y, Li D, Gao J. Shizhifang ameliorates pyroptosis of renal tubular epithelial cells in hyperuricemia through inhibiting NLRP3 inflammasome. J Ethnopharmacol. 2023;317:116777.
14. Shen B, Mei M, Ai S, Liao X, Li N, Xiang S, Wen C, Tao Y, Dai H. TRPC6 inhibits renal tubular epithelial cell pyroptosis through regulating zinc influx and alleviates renal ischemia-reperfusion injury. Faseb J. 2022;36(10):e22527.
15. Wang F, Huang M, Wang Y, Hong Y, Zang D, Yang C, Wu C, Zhu Q. Membrane attack complex C5b-9 promotes renal tubular epithelial cell pyroptosis in trichloroethylene-sensitized mice. Front Pharmacol. 2022;13:877988.
16. Liu B, Tu Y, Ni G, Yan J, Yue L, Li Z, Wu J, Cao Y, Wan Z, Sun W, et al. Total flavones of abelmoschus manihot ameliorates podocyte pyroptosis and injury in high glucose conditions by targeting METTL3-dependent m6A modification-mediated NLRP3-inflammasome activation and PTEN/PI3K/Akt signaling. Front Pharmacol. 2021;12:667644.
17. Wang X, Li Q, He S, Bai J, Ma C, Zhang L, Guan X, Yuan H, Li Y, Zhu X, et al. LncRNA FENDRR with m6A RNA methylation regulates hypoxia-induced pulmonary artery endothelial cell pyroptosis by mediating DRP1 DNA methylation. Mol Med (Cambridge Mass). 2022;28(1):1–126.
18. Meng Z, Cao R, Wang Y, Cao H, Liu T, Yang Z, Wang X. Suppression of renal TRPM7 may alleviate kidney injury in the renal transplantation. World J Urol. 2014;32(5):1303–11.
19. Mima A, Qi W, King GL. Implications of treatment that target protective mechanisms against diabetic nephropathy. Semin Nephrol. 2012;32(5):471–8.
20. Mima A. A narrative review of diabetic kidney disease: previous and current evidence-based therapeutic approaches. Adv Ther. 2022;39(8):3488–500.
21. Mima A. Sodium-glucose cotransporter 2 inhibitors in patients with non-diabetic chronic kidney disease. Adv Ther. 2021;38(5):2201–12.
22. Roignant JY, Soller M. M(6)A in mRNA: an ancient mechanism for fine-tuning gene expression. Trends Genet. 2017;33(6):380–90.
23. Gilbert WV, Bell TA, Schaening C. Messenger RNA modifications: form, distribution, and function. Science. 2016;352(6292):1408–12.
24. Suo L, Liu C, Zhang Q, Yao M, Ma Y, Yao J, Jiang Q, Yan B. METTL3-mediated N 6 -methyladenosine modification governs pericyte dysfunction during diabetes-induced retinal vascular complication. Theranostics. 2022;12(1):277–89.
25. Yang J, Liu J, Zhao S, Tian F. N(6)-methyladenosine METTL3 modulates the proliferation and apoptosis of Lens epithelial cells in diabetic cataract. Mol Ther Nucleic Acids. 2020;20:111–6.
26. Zhou J, Wei T, He Z. ADSCs enhance VEGFR3-mediated lymphangiogenesis via METTL3-mediated VEGF-C m(6)a modification to improve wound healing of diabetic foot ulcers. Mol Med. 2021;27(1):146.

27. Xu Z, Jia K, Wang H, Gao F, Zhao S, Li F, Hao J. METTL14-regulated PI3K/Akt signaling pathway via PTEN affects HDAC5-mediated epithelial-mesenchymal transition of renal tubular cells in diabetic kidney disease. Cell Death Dis. 2021;12(1):32.
28. Li M, Deng L, Xu G. METTL14 promotes glomerular endothelial cell injury and diabetic nephropathy via m6A modification of α-klotho. Mol Med. 2021;27(1).
29. Zhao X, Livingston MJ, Liang X, Dong Z. Cell apoptosis and autophagy in renal fibrosis. In. Singapore: Springer Singapore; 2019. pp. 557–84.
30. Fang L, Zhou Y, Cao H, Wen P, Jiang L, He W, Dai C, Yang J. Autophagy attenuates diabetic glomerular damage through protection of hyperglycemia-induced podocyte injury. PLoS ONE. 2013;8(4):e60546.
31. Qi C, Mao X, Zhang Z, Wu H, Carlos MS, Martinez Salgado C. Classification and differential diagnosis of diabetic nephropathy. J Diabetes Res. 2017;2017:8637137–8.
32. Mima A. Mitochondria-targeted drugs for diabetic kidney disease. Heliyon. 2022;8(2):e8878.
33. Wei S, Qiu T, Yao X, Wang N, Jiang L, Jia X, Tao Y, Wang Z, Pei P, Zhang J, et al. Arsenic induces pancreatic dysfunction and ferroptosis via mitochondrial ROS-autophagy-lysosomal pathway. J Hazard Mater. 2020;384:121390.
34. Mima A, Francesco C, Chiarelli F. Inflammation and oxidative stress in diabetic nephropathy: new insights on its inhibition as new therapeutic targets. J Diabetes Res. 2013;2013:248563–8.
35. Lin Q, Li S, Jiang N, Shao X, Zhang M, Jin H, Zhang Z, Shen J, Zhou Y, Zhou W, et al. PINK1-parkin pathway of mitophagy protects against contrast-induced acute kidney injury via decreasing mitochondrial ROS and NLRP3 inflammasome activation. Redox Biol. 2019;26:101254.
36. Ivankovic D, Chau KY, Schapira AH, Gegg ME. Mitochondrial and lysosomal biogenesis are activated following PINK1/parkin-mediated mitophagy. J Neurochem. 2016;136(2):388–402.

Publisher's note